LITHOS 398-399 (2021) 106280

Contents lists available at ScienceDirect

LITHOS

journal homepage: www.elsevier.com/locate/lithos

Research Article

Geochronology and Sr-Nd-Pb-Hf-O isotope geochemistry of Miocene intrusive rocks from Tsushima Islands, Japan: Constraints on petrogenesis and tectonic setting

Eun Ji Yi [a], Sung Hi Choi [a,b,*], Ji-In Kim [a], Jeong-Hyun Lee [a,b], Nak Kyu Kim [c]

[a] Department of Astronomy, Space Science and Geology, Chungnam National University, Daejeon 34134, South Korea
[b] Department of Geological Sciences, Chungnam National University, Daejeon 34134, South Korea
[c] Division of Earth Sciences, Korea Polar Research Institute, Incheon 21990, South Korea

ARTICLE INFO

Keywords:
Miocene intrusive rocks
Tsushima Islands
Sr-Nd-Pb-Hf-O isotopes
Zircon U-Pb age

ABSTRACT

We present geochemical and Sr-Nd-Pb-Hf-O isotopic data and zircon U-Pb ages for Miocene intrusive rocks (granitoids, mafic microgranular enclaves (MMEs), and diabases) from Tsushima Islands between Kyushu (Japan) and southeastern Korea. A granite yielded an age of 16.23 ± 0.16 Ma. The granitoids are mostly I-type, but are transitional between metaluminous and peraluminous compositions. All samples exhibit enrichment in LREE and LILE (e.g., K, Rb, and Pb), and depletion in HFSE (e.g., Nb, Ta, and Ti), implying formation in a subduction-related tectonic setting. However, on tectonic discrimination diagrams, data for all samples plot between the orogenic and anorogenic fields, indicating that Tsushima Islands were in a transitional tectonic regime from subduction to continental extension at ca. 16 Ma. The $\delta^{18}O_{clinopyroxene}$ values of a diabase range from 5.65‰ to 5.84‰. The Sr-Nd-Pb isotopic compositions of the diabases ($^{87}Sr/^{86}Sr$ = 0.70423–0.70481; ε_{Nd} = −0.8 to +3.6; $^{206}Pb/^{204}Pb$ = 18.27–18.40) are within the range of Miocene Eoil basalts from the Cenozoic Yangnam Basin in southeastern Korea, indicating the mantle source was a metasomatized mantle wedge. The granitoids are characterized by more enriched isotopic compositions than the diabases ($^{87}Sr/^{86}Sr$ = 0.70611–0.70756; ε_{Nd} = −6.0 to −3.8; $^{206}Pb/^{204}Pb$ = 18.43–18.55), and the MMEs have an intermediate isotopic composition. $\delta^{18}O_{quartz}$ values of the granitoids vary from 8.68‰ to 9.25‰, and zircons from a granite have $\varepsilon_{Hf}(t)$ values of −1.7 ± 1.2. The MMEs may have formed by partial melting of amphibolitic lower crust, whereas the granitoids possibly had a hybrid source consisting of amphibolite and graywacke.

1. Introduction

The East Sea (Sea of Japan) is a marginal basin that formed as a complex pull-apart basin in a dextral shear zone (the Yangsan/Tsushima-Goto faults between South Korea and Japan, and the Hidaka Shear Zone in Hokkaido, Japan) in the early to middle Miocene (Itoh, 2001; Jolivet and Tamaki, 1992; Lallemand and Jolivet, 1985/1986). It can be divided into three major, deep basins: the Japan, Yamato, and Ulleung basins (Fig. 1a). The Japan Basin comprises normal oceanic crust that is 6–7 km in thickness, and the Yamato Basin is considered twice as thick as extended island arc crust (Jolivet and Tamaki, 1992). The Ulleung Basin comprises thinned continental crust intruded by basaltic dikes (Choi, 2021; Itoh, 2001; Jolivet and Tamaki, 1992).

Paleomagnetic data suggest a rotation of southwest Japan has occurred with a Euler pole located near the Korea (i.e., Tsushima) Strait (34°N, 129°E; Jolivet and Tamaki, 1992; Otofuji et al., 1991). In addition to this clockwise rotation, a small counterclockwise rotation of west Kyusu, possibly associated with sinistral motion during the Cenozoic, may also have occurred, although its exact mechanism and age are controversial (e.g., Fabbri et al., 1996; Faure and Lalevée, 1987; Itoh, 2001; Jolivet and Tamaki, 1992). Northeast Japan underwent clockwise rotation during the opening of the East Sea around a pole located north of Hokkaido (38.5°N, 122°E; Jolivet and Tamaki, 1992; Otofuji et al., 1985). The arrival of the Philippine Sea Plate from the south (ca. 15 Ma) may have progressively stopped the opening of the East Sea (Jolivet and Tamaki, 1992).

The western margin of the East Sea is marked by the N20°*E*-trending transcurrent Tsushima-Goto fault system in the Korea Strait between

* Corresponding author at: Department of Astronomy, Space Science and Geology, Chungnam National University, Daejeon 34134, South Korea.
E-mail address: chois@cnu.ac.kr (S.H. Choi).

https://doi.org/10.1016/j.lithos.2021.106280
Received 24 March 2021; Received in revised form 2 June 2021; Accepted 2 June 2021
Available online 8 June 2021

South Korea and Kyushu (Fig. 1a–b), which had an important role during the opening of the East Sea (e.g., Fabbri et al., 1996). The displacement along the Tsushima-Goto fault system was polyphase: dextral motion during the early Miocene and sinistral motion during the middle Miocene (Fabbri et al., 1996; Kim et al., 2008). The compressional stress field in the middle Miocene is considered responsible for reactivation of the fault system as a sinistral–reverse fault (Fabbri et al., 1996).

The Miocene Tsushima intrusive rocks can provide important information for constraining the tectonic evolution of the western margin of the East Sea. A previous study (Shin et al., 2009) suggested that upwelling mantle might have provided the mafic melts and heat for the Tsushima intrusive rocks to form in an extensional tectonic regime. However, the study of Shin et al. (2009) was based mainly on petrographic and geochemical data obtained from the granitoids. In this paper, we present geochemical and geochronological data, including Sr-Nd-Pb-Hf-O isotopes and zircon U-Pb ages, for the Miocene Tsushima plutons (diabases and granitoids). The objective of this study was to constrain the petrogenesis and tectonic setting of this magmatism.

2. General geology

The Tsushima Islands are located between Kyushu (Japan) and southeastern Korea, and comprise mainly early Eocene to early Miocene sedimentary rocks (the Taishu Group) and Miocene igneous rocks (Fig. 1b). The Taishu Group is ~5400 m thick, and consists of deltaic to shallow marine mudstone, shale, and sandstone (Shin et al., 2009; Takahashi, 1969). It can be subdivided into Upper, Middle, and Lower formations. A thin lapilli tuff occurs at the boundary between the Middle and Lower formations. Zircon fission-track dating of the lapilli tuff yielded ages of 30.5 ± 2.5 to 18.7 ± 1.2 Ma (Takahashi and Hayashi, 1985, 1987).

The Tsushima igneous rocks comprise mainly granitic stocks and quartz porphyry dikes and sheets, with minor amounts of diabase dikes intruding the sedimentary rocks after or during the final stage of deformation of the Taishu Group (Kim et al., 2008; Shin et al., 2009). A thermal metamorphic aureole, with an average width of 800 m, occurs around the granitic intrusion (Ikemi et al., 2001; Kim et al., 2008; Shin et al., 2009). The intrusion depth of the granitoid is estimated at 2–6 km (Shin et al., 2009). Fission-track data for zircons from a dacite and quartz porphyry record ages of 18.7 ± 1.0 to 16.9 ± 1.0 Ma and 14.8 ± 0.8 to 14.2 ± 0.7 Ma, respectively (Takahashi and Hayashi, 1985, 1987). Hornblende K-Ar ages of the granites are 17.4 ± 0.4 to 13.6 ± 0.4 Ma (Ikemi et al., 2001), and zircon fission-track ages of 14.9 ± 0.8 Ma (Takahashi and Hayashi, 1985) and 16.5 ± 1.6 to 12.8 ± 1.4 Ma (Ishikawa and Tagami, 1991) have been reported for the granites. The

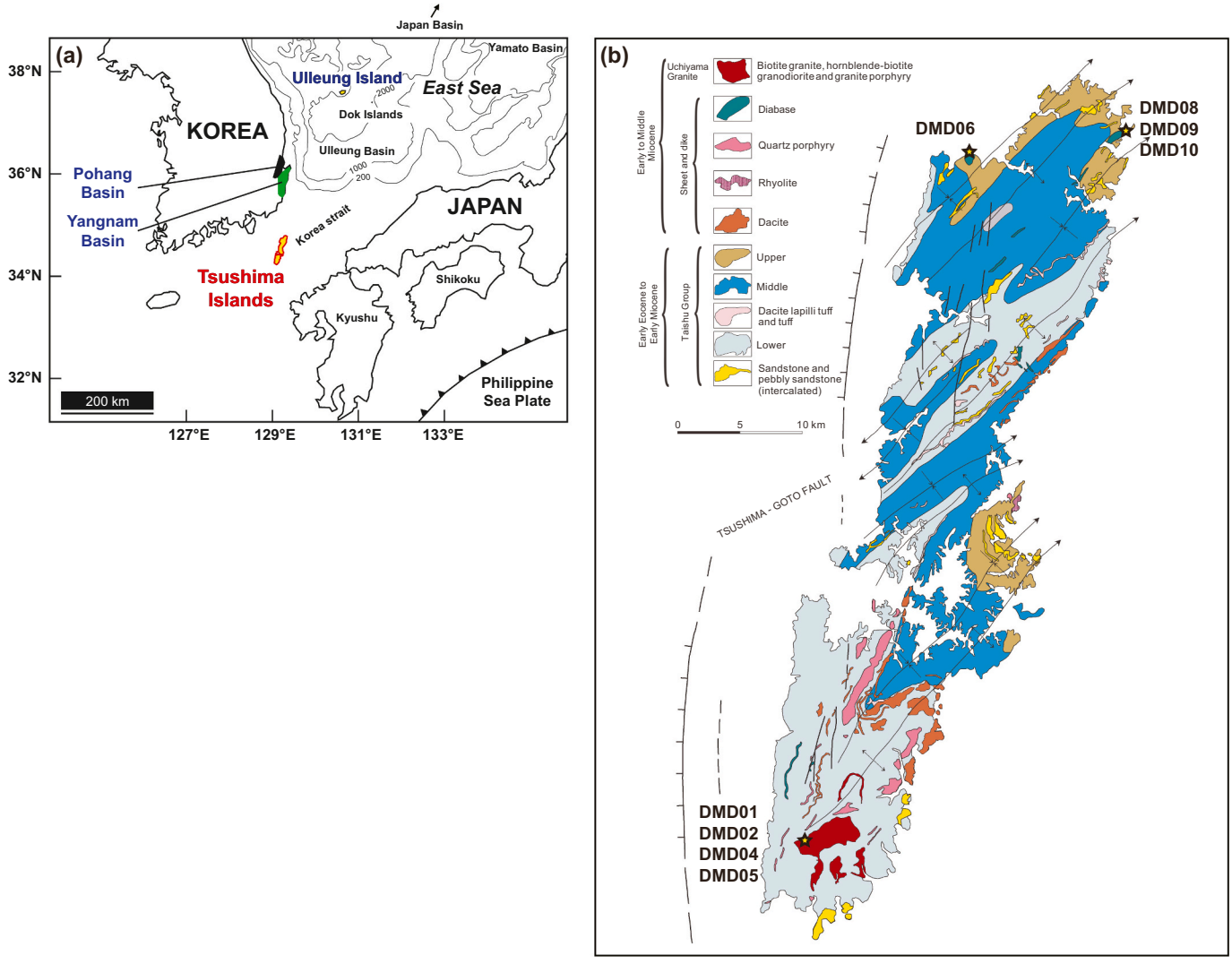

Fig. 1. (a) Regional map showing Tsushima Islands (study area), and nearby Pohang Basin, Yangnam Basin, and Ulleung Island. (b) Geological map of Tsushima Islands showing the sample locations (modified after Takahashi, 1992).

diabases are considered to have been intruded at the same time as the silicic intrusions (Matsumoto and Takahashi, 1987). Vein-type Pb-Zn ore deposits (ca. 15 Ma) are developed along fracture zones in sedimentary rocks around the granites (Ikemi et al., 2001).

The paleo-stress field on the Tsushima Islands during the late Oligocene to early Miocene was a NNE-SSW- to NW-SE-oriented extensional regime (Fabbri et al., 1996; Kim et al., 2008). However, this changed progressively to a NW-SE-oriented shortening regime during the middle Miocene (Fabbri et al., 1996). NE–SW- to NNE–SSW-trending fold axes are pervasive at Tsushima, which are thought to have formed before the silicic intrusions, and may have been related to the clockwise rotation of southwest Japan (Ishikawa and Tagami, 1991; Kim et al., 2008) or sinistral movement on the Tsushima-Goto Fault (Fabbri et al., 1996).

3. Petrography

The Miocene Tsushima intrusive rocks consist of granitoids and diabases. The granitoids contain mafic microgranular enclaves (MMEs) of various sizes, which are up to a few meters in diameter (Ishihara and Imai, 2000; Shin et al., 2009 and references therein). The enclaves are mostly rounded to ovoid in shape, but some have crenulated to cuspate boundaries, indicating magma mingling (Ishihara and Imai, 2000). Miarolitic cavities containing hornblende, tourmaline, titanite, quartz, or zeolite are often observed in the granites (Shin et al., 2009). We selected nine samples for this study, four of which are granitoids (DMD01, 02H, 04, 05), one is an MME (DMD02ME), and four are diabases (DMD06, 08, 09, 10). The granitoids were sampled in Ayumodoshi National Park, Uchiyama, Izuhara town, Tsushima City. The diabases were sampled in Sago-Kitasato (DMD06), Kami-Agata town, and Nishi-domari (DMD08, 09, 10), Kami-Tsushima town, Tsushima City.

Modal analysis was conducted on thin-sections by point-counting: ~800 to 1000 points for granitoids and MME samples, and ~ 500 to 900 points for diabase samples (Table S1). The results are shown in a quartz-alkali feldspar-plagioclase (QAP) classification diagram (Fig. S1). Samples DMD01, DMD04, and DMD05 plot in the granite field, and sample DMD02H in the granodiorite field. These samples are hereafter referred to as the Tsushima granitoids. They have porphyritic textures with plagioclase, quartz, and K-feldspar phenocrysts (>1 mm) set in a groundmass of quartz, plagioclase, K-feldspar, biotite, and opaque minerals (0.1–1.0 mm; Fig. S2a). Sample DMD05 contains perthite phenocrysts (>1 mm; Fig. S2b).

The MME sample (DMD02ME) plots in the tonalite field (Fig. S1). It consists of quartz, K-feldspar, plagioclase, biotite, hornblende, and opaque minerals (0.1–0.5 mm) with an equigranular texture (Fig. S2c). It is fine-grained in comparison to the host granitoids. The MMEs are crenulated or rounded in shape with a chilled margin.

The diabase samples (DMD06, DMD08, DMD09, and DMD10) plot in the (quartz) diorite and (quartz) gabbro fields (Fig. S1). They consist of plagioclase, clinopyroxene, biotite, chlorite, epidote, quartz, and calcite (Fig. S2d-f). The chlorite, epidote, quartz, and calcite are secondary minerals produced by alteration. Alteration of plagioclase to sericite is also common.

4. Analytical methods

Ion microprobe zircon U-Pb dating was conducted on one granite sample (DMD01) at the Korea Basic Science Institute (KBSI) in Ochang, South Korea. Prior to analysis, zircons were separated from the crushed sample by conventional techniques, including magnetic and heavy liquid methods. The separated grains were mounted in epoxy resin with zircon standards SL13 and FC1, and then polished to expose grain mid-sections for age dating. Cathodoluminescence (CL) and back-scattered electron (BSE) images of the analyzed zircons were obtained by scanning electron microscopy (SEM; JEOL 6610LV). The identification of zircon and its inclusions was conducted with an Oxford INCA X-act energy dispersive spectrometer. The analytical procedures followed those of Williams (1998). Concentrations of U and Th were calculated with reference to SL13 (U = 238 ppm). The measured $^{206}Pb/^{238}U$ ratios were calibrated using the FC1 zircon ($^{206}Pb^*/^{238}U$ = 0.1859; age = 1099 Ma; Paces and Miller Jr., 1993). Common Pb corrections and age calculations were performed using Squid 2.50 and Isoplot 3.71 software (Ludwig, 2008, 2009). With the exception of zircons with ages of >1200 Ma, most weighted-mean ages were calculated using ^{207}Pb-corrected $^{206}Pb/^{238}U$ ratios. Calculated age data are reported at the 95% confidence level in Table S2.

In situ zircon Hf isotopic compositions were determined using a laser ablation multiple-collector inductively coupled plasma mass spectrometer (LA-MC-ICP-MS), which comprises an ESI NWA193^{UC} LA system and a Nu Plasma II MC-ICP-MS, at the KBSI. The Hf isotopic data were obtained from the same sites used for U—Pb age dating. The spot size was 50 μm and the energy density was 5.2 J/cm^2. Details of the analytical methods are given in Kim et al. (2019b). To evaluate the precision and accuracy of the $^{176}Hf/^{177}Hf$ ratios, two standard zircons (91500 and FC1) were analyzed at the beginning and end of the analytical session, and repeatedly at regular intervals throughout. Standard zircons 91,500 and FC1 yielded average $^{176}Hf/^{177}Hf$ ratios of 0.282298 ± 0.000015 (N = 30; 2σ) and 0.282189 ± 0.000024 (N = 14; 2σ), which are consistent with the recommended values of 0.282313 ± 0.000012 and 0.282183 ± 12 for these standards, respectively (Fisher et al., 2014). All obtained ratios are presented with 2σ errors, and data reduction was conducted with Iolite 2.5 software (Paton et al., 2011).

For whole-rock geochemical analysis, fresh rock samples were selected and crushed into <0.5-cm-size pieces in a tungsten carbide mortar. Subsequently, the fragments were powdered with an agate ball mill. Whole-rock major and trace element concentrations were obtained with lithium metaborate/tetraborate fusion inductively coupled plasma (FUS-ICP) and inductively coupled plasma mass spectrometry (ICP-MS) techniques, respectively, at Act Labs, Ontario, Canada. Standards BIR-1, W-2, and DNC-1 were analyzed to assess analytical accuracy. The precision of the standard data was ±5% for major elements and ± 10% for trace elements. The results are given in Table S3.

The chemical separation of Sr, Nd, and Pb for whole-rock isotopic analysis was performed at Chungnam National University in Daejeon, South Korea, using procedures described previously (Choi et al., 2013). Analyses of Sr, Nd, and Pb isotopes were conducted using a VG Sector thermal ionization mass spectrometer (TIMS) at the KBSI. The $^{87}Sr/^{86}Sr$ and $^{143}Nd/^{144}Nd$ ratios were corrected for instrumental mass fractionation by normalizing to $^{86}Sr/^{88}Sr = 0.1194$ and $^{146}Nd/^{144}Nd = 0.7219$, respectively. Replicate analysis of NBS-987 and JNdi-1 standards yielded $^{87}Sr/^{86}Sr = 0.710257 \pm 0.000003$ (N = 15; 2σ) and $^{143}Nd/^{144}Nd = 0.512110 \pm 0.000009$ (N = 14; 2σ). Measured Pb isotopic ratios were corrected for instrumental mass fractionation of 0.1% amu^{-1} by reference to replicate analyses of the standard NBS-981. Total procedure blanks were averaged at 30 pg for Sr and Nd, and 50 pg for Pb. The results are given in Table S3.

For analysis of O isotopes, ultrapure quartz and clinopyroxene grains were separated by handpicking under a binocular microscope, which yielded clear grains free of any visible minerals or fluid inclusions. Oxygen isotope analysis was performed at the Korea Polar Research Institute (KOPRI) using a laser fluorination system (Kim et al., 2019a, 2019b). Aliquots of about 2 mg were loaded in a Ni sample holder and placed in the reaction chamber. For laser fluorination, the sample was heated with a 25 W CO_2 laser in the presence of sufficient BrF_5. Subsequently, the liberated O_2 was purified by a series of purification steps. The isotopic composition of the purified O_2 was analyzed using a dual-inlet mass spectrometer. The measured $^{18}O/^{16}O$ ratios were normalized to VSMOW (Vienna Standard Mean Ocean Water) and expressed in δ-notation defined as $\delta^{18}O$ (‰) = 1000 × $[(^{18}O/^{16}O)_{sample}/(^{18}O/^{16}O)_{VSMOW} - 1]$. The Light Antarctic Precipitation standard (SLAP) was measured, and the VSMOW-SLAP scaling was applied to reduce

inter-laboratory differences (Gonfiantini, 1978). The measured $\delta^{18}O$ value relative to VSMOW of SLAP was −54.48‰ ± 0.15‰ (n = 8; 1σ), and was thus normalized to −55.50‰ to obtain the scaling factor. Based on the results of standard water analysis, we normalized our data by applying the 1.019 scaling factor and the VSMOW-SLAP scaling method proposed by Kusakabe and Matsuhisa (2008). The results are listed in Table S4.

5. Results

5.1. Zircon geochronology

Zircons from sample DMD01 were dated. Representative CL images of the zircon grains are shown in Fig. S3. Results of the zircon U-Pb analyses are listed in Table S2, and shown on Terra–Wasserburg diagrams in Fig. 2.

The zircons are transparent, pale brown, euhedral–subhedral with sharp prismatic terminations, and range from 40 to 230 μm in size. The CL imaging revealed magmatic oscillatory or sector zoning. Some grains contain inclusions of alkali feldspar, biotite, quartz, or apatite. Some zircons had unzoned dark inherited cores. The U-Pb analyses were carried out mainly on the magmatic zircon domains. Uranium concentrations vary from 73 to 1814 ppm, with Th/U ratios of 0.25–1.57 (Table S2). The weighted-mean ^{207}Pb-corrected $^{206}Pb/^{238}U$ age is 16.23 ± 0.16 Ma (n = 17; MSWD = 2.1; Fig. 2), which is within the age range determined by hornblende K-Ar and zircon fission-track methods for the Tsushima granites (Ikemi et al., 2001; Ishikawa and Tagami, 1991). Also listed in Table S2 are six data-points for inherited zircon cores, which have scattered ages from Paleoproterozoic to Jurassic (2.39–0.16 Ga), but were not plotted in Fig. 2 for clarity.

5.2. Whole-rock major and trace element data

Whole-rock major and trace element data are listed in Table S3. The loss-on-ignition (LOI) values for granitoids are lower than 1%, but for diabases, it is in range of 4–6% due to weathering (Table S3). The data were plotted on a total alkalis vs. silica (TAS) classification diagram (Fig. 3a). All samples belong to the sub-alkaline series. The Tsushima diabases are basalt to basaltic andesite in composition. The Tsushima granitoids are compositionally dacite to rhyolite, and the MME is an andesite. Using the K_2O vs. SiO_2 nomenclature of Le Maitre et al. (1989) (Fig. 3b), the diabases and MME belong to the medium-K calc-alkaline series, but the granitoids are part of the high-K calc-alkaline series. The

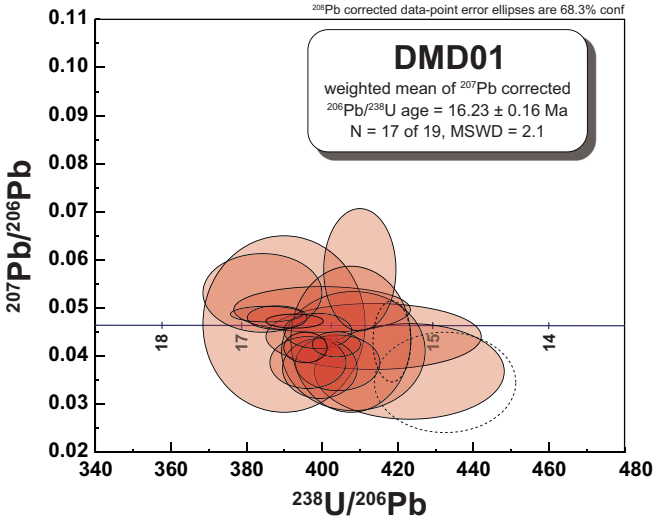

Fig. 2. Tera–Wasserburg concordia diagram for zircons from a Tsushima granite (sample DMD01). The data-point error ellipses are 1σ errors.

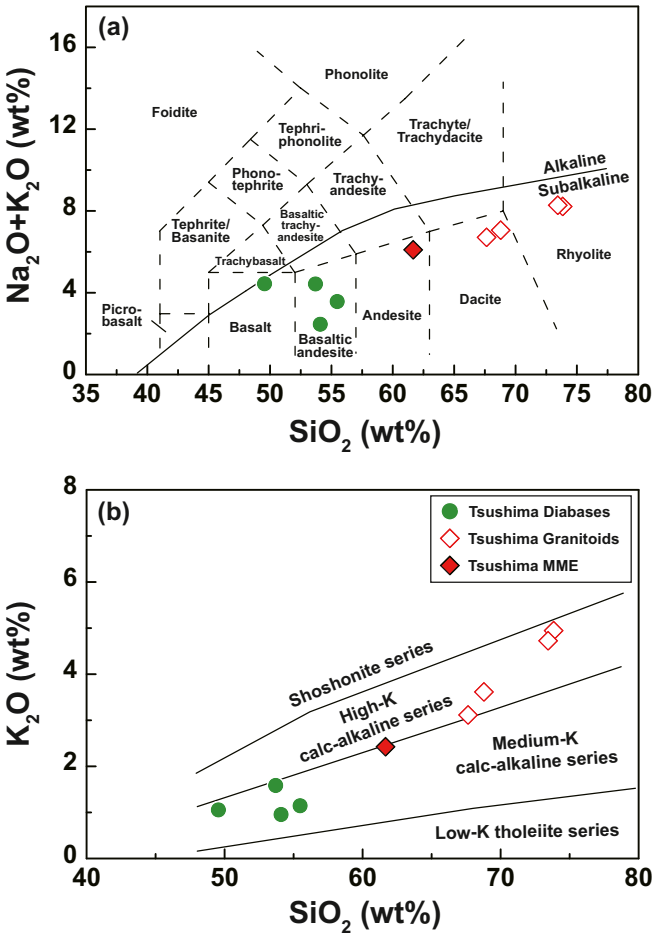

Fig. 3. Classification of the Tsushima intrusive rocks: (a) SiO_2 vs. $Na_2O + K_2O$ and (b) SiO_2 vs. K_2O. The fields are from Le Maitre et al. (1989). The boundary line dividing the alkaline and sub-alkaline series in (a) is from Irvine and Baragar (1971).

alumina saturation index (A/CNK = molar $Al_2O_3/[CaO + Na_2O + K_2O]$) values of the studied granitoids and MME range from 0.91–1.04, and are metaluminous to weakly peraluminous, and defined as being mostly I-type with some S-type compositions (Fig. S4).

Major element and representative trace element concentrations are plotted in Figs. 4 and S5, respectively, as a function of SiO_2. Also shown in these plots are published data for Tsushima intrusive rocks. The Tsushima diabases have SiO_2 and MgO contents ranging from 49.6 to 55.5 and 4.6 to 7.1 wt%, respectively, with Mg# (100 Mg/[Mg + Fe^{2+}]) of 54.3–61.6 (Table S3). MgO, Fe_2O_3*, CaO, Al_2O_3, TiO_2, Na_2O, P_2O_5, and MnO contents decrease with increasing SiO_2, but K_2O increases (Fig. 4). The diabases have Ni and Co contents that vary from 38 to 102 and 24 to 32 ppm, respectively (Table S3). The Ni, Co, Cr, Sr, and Eu contents decrease with increasing SiO_2, implying fractional crystallization of olivine, clinopyroxene, and plagioclase, but Zr, Rb, and Ba increase with increasing SiO_2 (Fig. S5a-d). The MME has 61.7 wt% SiO_2 and 2.4 wt% MgO, with Mg# = 36.7. The granitoids have elevated SiO_2 (67.6–73.8 wt%), but lower MgO (0.3–1.0 wt%) contents compared with the diabases. MgO, Fe_2O_3*, CaO, Al_2O_3, TiO_2, Na_2O, P_2O_5, and MnO contents of the granitoids decrease with increasing SiO_2, but K_2O increases (Fig. 4). The Ni contents are below the detection limit (20 ppm; Table S3). The Co, Cr, Sr, Eu, V, and Zr contents of the granitoids decrease with increasing SiO_2, but Rb and Ba increase (Fig. S5a-i). In general, data for the MME plot along the liquid line of descent for the granitoids to less evolved compositions. However, the diabases do not show coherent geochemical trends with the granitoids and MME,

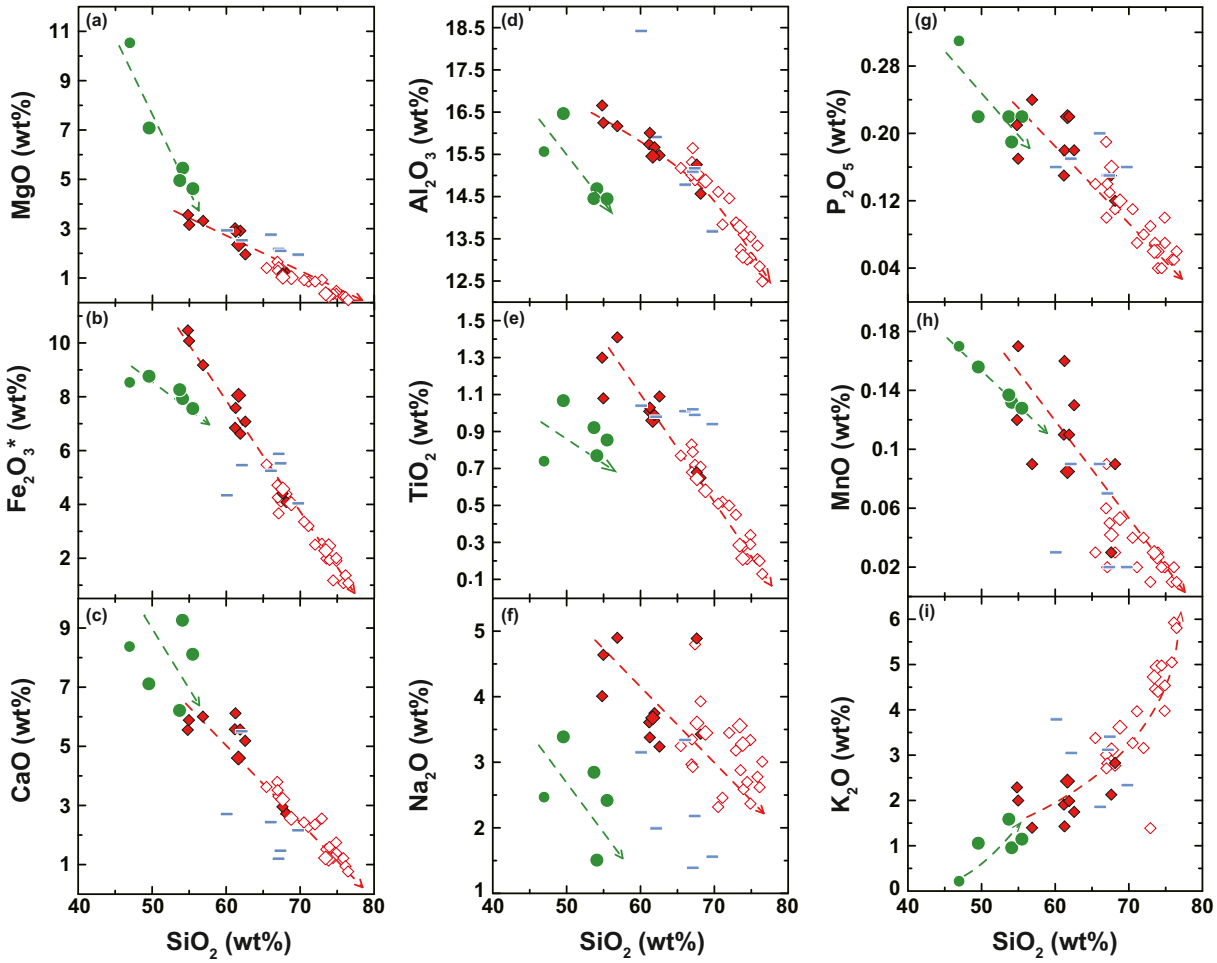

Fig. 4. Major element variation diagrams for the Tsushima intrusive rocks. Symbols are as in Fig. 3. Small symbols are data from the literature Tsushima intrusions (Shin et al., 2009). Also shown for comparison are data for the Taishu Group sedimentary rocks (–, Shin et al., 2009).

indicating their non-cogenetic nature. The diabases and MME are sodic in nature (K_2O/Na_2O = 0.31–0.66 by weight), whereas K_2O/Na_2O = 0.87–1.51 for the granites (Table S3).

Chondrite-normalized rare earth element (REE) patterns are shown in Fig. 5a–b. The Tsushima diabases exhibit enrichment in light REEs (LREEs), with $(La/Yb)_N$ = 3.6–4.9 (Table S3) and no Eu anomalies. The MME and granitoids also have LREE-enriched patterns with $(La/Yb)_N$ of 5.7 and 3.0–8.1, respectively, but the granitoids are characterized by pronounced negative Eu anomalies (Fig. 5b). Primitive-mantle-normalized trace element patterns are shown in Fig. 5c–d, along with compositions for typical ocean island basalt (Sun and McDonough, 1989) and average oceanic arc basalt (Kelemen et al., 2003). The Tsushima samples exhibit an arc-like enrichment in large-ion lithophile elements (LILEs), such as Cs, Rb, U, K, and Pb, and depletion in high-field-strength elements (HFSEs), such as Nb and Ta. Pronounced negative Sr, P, and Ti anomalies for the granitoids indicate fractional crystallization of plagioclase, apatite, and titanomagnetite, respectively.

5.3. Sr-Nd-Pb-Hf-O isotopes

Whole-rock Sr-Nd-Pb isotopic data for the Tsushima intrusive rocks are listed in Table S3 and shown in Figs. 6–7. The mantle end-member compositions of depleted MORB mantle (DMM), enriched mantle type 1 (EM1) and type 2 (EM2; Zindler and Hart, 1986), and fields for mid-ocean ridge basalts (MORBs) are shown for comparison in the plots. Also shown are published data for the Tsushima intrusive rocks (Shin et al., 2009). The Sr-Nd-Pb isotopic compositions of the Tsushima diabases show little variation, with $(^{87}Sr/^{86}Sr)_t$ = 0.70423–0.70481, $(^{143}Nd/^{144}Nd)_t$ = 0.512574–0.512803, $\varepsilon_{Nd}(t)$ = −0.8 to +3.6, $^{206}Pb/^{204}Pb$ = 18.27–18.40, $^{207}Pb/^{204}Pb$ = 15.58–15.60, and $^{208}Pb/^{204}Pb$ = 38.52–38.65 (Table S3). The limited range of isotopic compositions indicates that the element mobility was not significant during secondary alteration processes. The Tsushima granitoids have more radiogenic Sr and Pb, and less radiogenic Nd, with $(^{87}Sr/^{86}Sr)_t$ = 0.70611–0.70756, $(^{143}Nd/^{144}Nd)_t$ = 0.512278–0.512420, $\varepsilon_{Nd}(t)$ = −6.6 to −3.8, $^{206}Pb/^{204}Pb$ = 18.43–18.55, $^{207}Pb/^{204}Pb$ = 15.61–15.64, and $^{208}Pb/^{204}Pb$ = 38.71–38.99 (Table S3). The MME has $(^{87}Sr/^{86}Sr)_t$ = 0.70612, $(^{143}Nd/^{144}Nd)_t$ = 0.512448, $\varepsilon_{Nd}(t)$ = −3.3, $^{206}Pb/^{204}Pb$ = 18.52, $^{207}Pb/^{204}Pb$ = 15.64, and $^{208}Pb/^{204}Pb$ = 38.91 (Table S3). In the Sr-Nd isotope plot (Fig. 6), all samples plot outside the MORB field, and fall approximately on a mixing array between MORB and Bulk Silicate Earth (BSE), and the EM2 component. In Pb isotope space (Fig. 7a–b), the samples plot above the Northern Hemisphere reference line (NHRL; Hart, 1984). On a $^{208}Pb/^{204}Pb$ vs. $^{206}Pb/^{204}Pb$ plot (Fig. 7b), they plot close to the upper limit of the Indian MORB field. The samples plot close to enriched mantle components on the $^{207}Pb/^{204}Pb$ vs. $^{206}Pb/^{204}Pb$ diagram (Fig. 7a). The Tsushima granitoids have more enriched Sr-Nd isotopic compositions than the MME, but are indistinguishable in Pb isotopic composition (Figs. 6–7).

Zircon Hf isotope analysis was undertaken at 18 spots that were U-Pb dated (Table S2). The 15 spots with $^{206}Pb/^{238}U$ ages of ca. 16 Ma have $^{176}Hf/^{177}Hf$ = 0.282547–0.282823, with $\varepsilon_{Hf}(t)$ = −7.6 to +2.1. The weighted-mean of the $^{176}Hf/^{177}Hf$ ratios is 0.282701 ± 0.000037 (n = 15; 2σ) with $\varepsilon_{Hf}(t)$ = −1.7 ± 1.2. Three analyses of

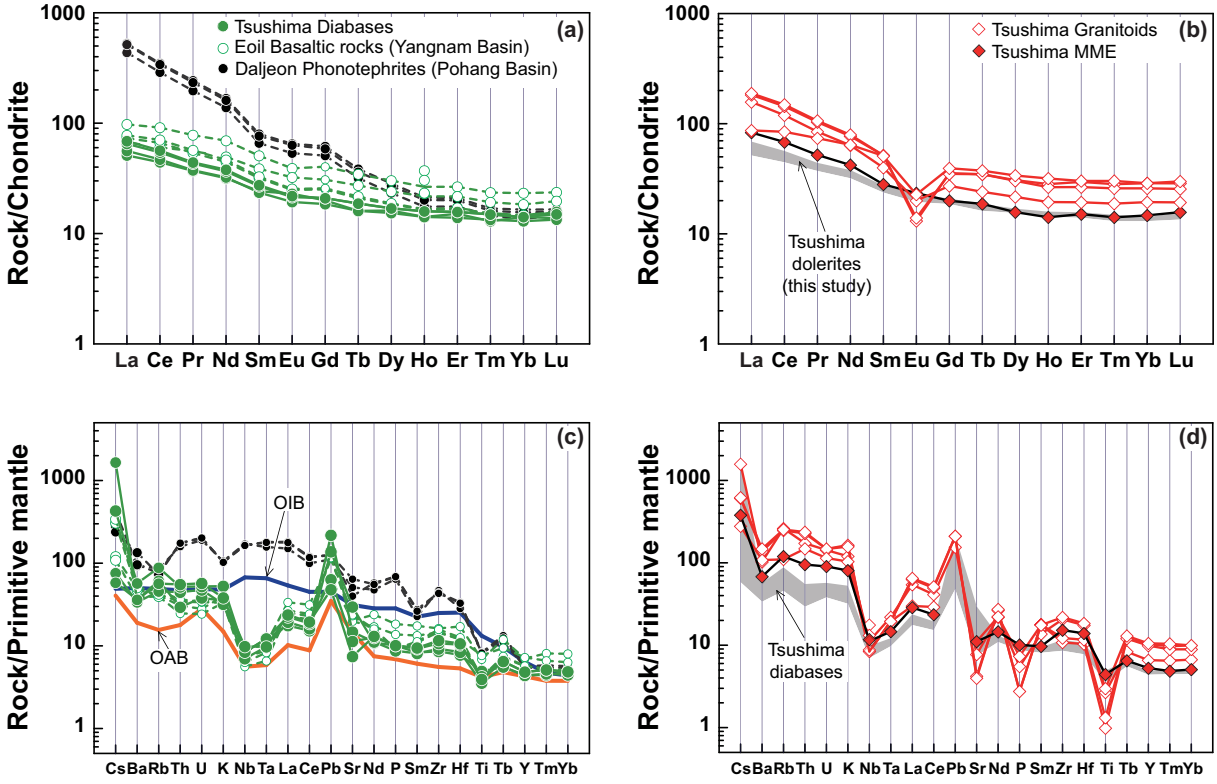

Fig. 5. (a–b) Chondrite-normalized rare earth element patterns and (c–d) primitive-mantle-normalized trace element patterns (normalizing values are from Sun and McDonough, 1989). Also shown are data for the Miocene Eoil basaltic rocks from Yangnam Basin and Daljeon phonotephrites from Pohang Basin, southeastern Korea (Choi et al., 2013), typical ocean island basalts (OIBs; Sun and McDonough, 1989), and average oceanic arc basalts (OABs; Kelemen et al., 2003).

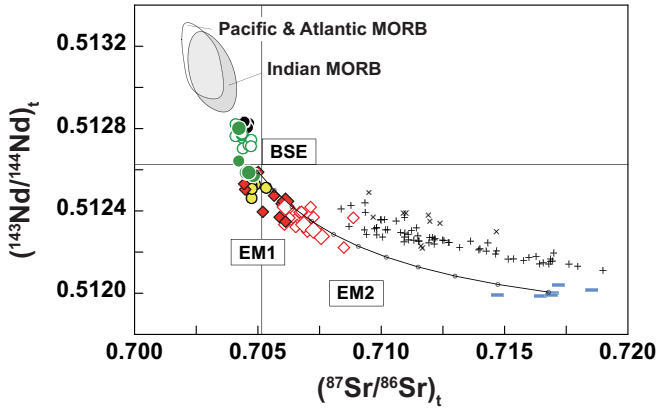

Fig. 6. Initial $^{143}Nd/^{144}Nd$ vs. $^{87}Sr/^{86}Sr$ ratios for the Tsushima intrusive rocks. The curved line is a reference binary mixing line between the most depleted MME sample (Sr = 281 ppm; Nd = 18.7 ppm; $^{87}Sr/^{86}Sr = 0.7050$; $^{143}Nd/^{144}Nd = 0.51259$; Shin et al., 2009) and the average composition of the Taishu Group sedimentary rocks (Sr = 148 ppm; Nd = 30.3 ppm; $^{87}Sr/^{86}Sr = 0.7161$; $^{143}Nd/^{144}Nd = 0.51199$; Shin et al., 2009). Symbols are as in Figs. 4 and 5. Data sources: Tsushima intrusive rocks and Taishu Group sedimentary rocks (Shin et al., 2009); Eoil basaltic rocks from the Yangnam Basin and Daljeon phonotephrites from the Pohang Basin (Choi et al., 2013 and references therein); Quaternary trachybasalts from Ulleung Island (yellow closed circles; Tatsumoto and Nakamura, 1991; Choi et al., 2006); mid-ocean ridge basalts (MORBs; Choi et al., 2013 and references therein); pelagic sediments from the East Sea and abyssal plain, east of Japan (×, Cousens et al., 1994), and Philippine Sea (+, Saitoh et al., 2015). Abbreviations: BSE = bulk silicate Earth; EM1 and EM2 = enriched mantle types 1 and 2, respectively (Zindler and Hart, 1986). (For interpretation of the references to colour in this figure legend, the reader is referred to the web version of this article.)

Proterozoic–Paleozoic inherited zircon cores (2387, 1882, and 563 Ma; Table S2) have $^{176}Hf/^{177}Hf = 0.281980–0.282470$, with $\varepsilon_{Hf}(t) = +1.3$ to $+31.3$.

Minerals such as clinopyroxene and quartz generally provide a more robust constraint on the O isotopic compositions of melts than whole-rocks, due to post-magmatic alteration of groundmass (Eiler et al., 2000). Thus, we obtained the O isotopic compositions of clinopyroxene and quartz in the Tsushima diabases and granites, respectively (Table S4). $\delta^{18}O_{clinopyroxene}$ values range from 5.65‰ to 5.84‰, similar to normal mantle-derived clinopyroxene (5.6‰ ± 0.2‰; Eiler et al., 1997; Mattey et al., 1994). $\delta^{18}O_{quartz}$ values range from 8.68‰ to 9.25‰.

6. Discussion

6.1. Petrogenesis of the Tsushima diabases

It is important to investigate the role of crustal contamination before characterizing the nature of the mantle source of the Tsushima diabases. The addition of crustal materials to basaltic magmas is expected to produce a positive $^{87}Sr/^{86}Sr$ and negative $^{143}Nd/^{144}Nd$ correlation with an index of fractionation such as Mg#. However, the Tsushima diabases do not show meaningful correlations between Mg# and Sr or Nd isotopic compositions (Fig. S6). The Tsushima diabases also have Sr–Nd–Pb isotopic compositions that plot within the oceanic basalt field in Sr-Nd and Pb-Pb isotope diagrams (Figs. 6–7). The Tsushima diabases have $\delta^{18}O_{clinopyoroxene} = +5.7‰$ to $+5.8‰$. Assuming O isotopic fractionation between pyroxene and basalt of −0.2‰ (Zhao and Zheng, 2003), these values correspond to whole-rock or magma values of +5.9‰ to +6.0‰. The $\delta^{18}O$ value of the upper mantle is +5.5‰ ± 0.4‰ (Mattey et al., 1994; Valley, 2003). Thus, the $\delta^{18}O$ values preclude significant crustal contamination of the Tsushima diabases.

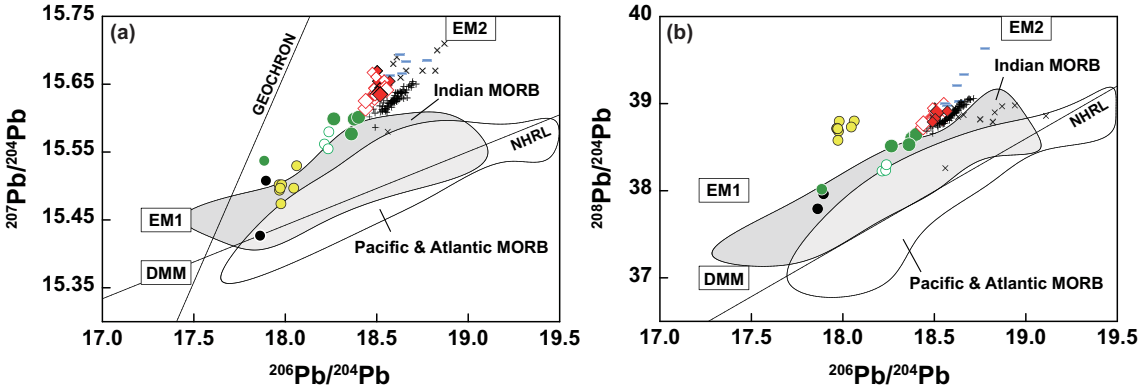

Fig. 7. Plots of (a) $^{207}Pb/^{204}Pb$ vs. $^{206}Pb/^{204}Pb$ and (b) $^{208}Pb/^{204}Pb$ vs. $^{206}Pb/^{204}Pb$ for the Tsushima intrusive rocks. The NHRL is the Northern Hemisphere reference line of Hart (1984). Symbols, data sources, and abbreviations are as in Fig. 6. DMM = depleted MORB mantle.

To identify the mantle source characteristics of the Tsushima diabases, we compared our data with middle Miocene basaltic rocks from Cenozoic basins in the southeastern Korean Peninsula, such as the Eoil basaltic rocks (22–16 Ma) from the Yangnam Basin and Daljeon phonotephrites (15–13 Ma) from the Pohang Basin (Figs. 5-7; Choi et al., 2013). These basins are considered to have formed with the opening of the East Sea (e.g., Chough et al., 2000). We also compared the Sr-Nd-Pb isotopic compositions of Quaternary intraplate trachybasalts from Ulleung Island in the East Sea (Choi et al., 2006) (Figs. 6–7).

Unlike the Tsushima diabases, the Daljeon phonotephrites have highly fractionated $(La/Yb)_N$ ratios without arc-like depletions in HFSEs and enrichments in LILEs (Fig. 5a, c). They also have more depleted Sr-Nd and less radiogenic Pb isotopic compositions compared with the Tsushima diabases (Figs. 6–7). Based on trace element patterns, Choi et al. (2013) argued that hydrous phase-bearing, metasomatized lithospheric mantle might have been the source for the Daljeon phonotephrites. However, our trace element data, along with the absence of primary biotite or calcite in our samples, suggest that metasomatized subcontinental lithospheric mantle was not the dominant source of the Tsushima diabases.

The Eoil basalts are similar to the Tsushima diabases in that they have arc-like trace element patterns (Fig. 5c). They also have similar REE patterns (Fig. 5a). Furthermore, the Eoil basalts have Sr-Nd-Pb isotopic compositions that plot in the field defined by the Tsushima diabases (Figs. 6–7). The geochemical characteristics of island arc basalts can be attributed to two main source components: the mantle wedge and subducting oceanic slab. High Sr/Y (>40) and La/Yb (>20) ratios have been regarded a typical feature of slab melts (e.g., Defant and Drummond, 1990). The Sr/Y and La/Yb ratios of the Tsushima diabases range from 7 to 31 and 5 to 7, respectively (Table S3), ruling out the possibility of slab-derived melts. The composition of the pristine mantle wedge prior to modification by subduction is close to that of depleted upper mantle (i.e., the MORB source). However, the mantle wedge of an active subduction zone can be overwhelmingly modified by slab-derived fluids/melts (e.g., McCulloch and Gamble, 1991; Tatsumi and Hanyu, 2003). Enrichment in LILEs relative to HFSEs is attributed to mantle wedge metasomatism by slab-derived fluids (e.g., McCulloch and Gamble, 1991; Perfit et al., 1980; Zheng, 2019). The Tsushima diabases have more enriched Sr-Nd-Pb isotopic compositions than MORBs (Figs. 6–7). Based on Nd-Hf isotopic decoupling, Choi et al. (2013) argued that the Eoil basalts were sourced from a mantle wedge metasomatized by the addition of subducted pelagic sediment-derived melts. Although no Hf isotope data have been obtained for the Tsushima diabases, the geochemical similarity between these two middle Miocene igneous units allows us to conclude that melting of a weakly metasomatized mantle wedge generated the Tsushima diabases.

The Ulleung trachybasalts are characterized by OIB-like trace element patterns, such as enrichments in LREEs and no depletions in HFSEs (Choi et al., 2006). This observation, and their emplacement through highly attenuated continental crust, led Choi et al. (2006) to suggest that the Ulleung volcanism were sourced from the asthenospheric mantle. The Ulleung basalts have EM1-like enriched Sr-Nd isotopic compositions compared with the Tsushima diabases (Fig. 6). On a plot of $^{207}Pb/^{204}Pb$ vs. $^{206}Pb/^{204}Pb$ (Fig. 7a), the Ulleung samples fall within the range of Indian MORBs. However, they are characterized by more radiogenic $^{208}Pb/^{204}Pb$ at a given $^{206}Pb/^{204}Pb$ (Fig. 7b) compared with Indian MORBs. In this respect, they are different from the Tsushima diabases that fall in the Indian MORB field on a plot of $^{208}Pb/^{204}Pb$ vs. $^{206}Pb/^{204}Pb$ (Fig. 7b), but which have more radiogenic Pb in $^{207}Pb/^{204}Pb$–$^{206}Pb/^{204}Pb$ space (Fig. 7a). Thus, it appears that the Tsushima diabases were not formed by upwelling asthenosphere in an intraplate tectonic setting.

6.2. *Petrogenesis of the Tsushima granitoids*

The Tsushima granitoids exhibit pronounced negative Nb and Ta anomalies (Fig. 5d), which are a diagnostic feature of igneous rocks formed in destructive margin settings or from a crustal source (e.g., Whalen et al., 1996). The $\varepsilon_{Nd}(t)$ values of the Tsushima granitoids range from −6.6 to −3.3 (Table S3). Zircons from a granite have $\varepsilon_{Hf}(t)$ values of -1.7 ± 1.2 (Table S2). The negative $\varepsilon_{Nd}(t)$ and $\varepsilon_{Hf}(t)$ values indicate reworking of an old crustal component, although it is difficult to rule out a mantle contribution. The occurrence of Paleoproterozoic to Jurassic inherited zircon cores in the Tsushima granite also suggests that melting of old crustal rocks had a dominant role in their generation.

Experimental data have shown that partial melting of mafic lower crust can generate metaluminous granitic melts (e.g., Karsli et al., 2007 and references therein). I-type granitoids would be produced by dehydration melting of intermediate to mafic source rocks (Vielzeuf et al., 1990). To identify specific source materials for the Tsushima granitoids, major element compositions of melts produced experimentally by dehydration melting of a wide range of metamorphic rocks (amphibolite, graywacke, and pelite) are shown in Fig. 8. Low $Al_2O_3/(FeO + MgO + TiO_2)$ ratios and high $Al_2O_3 + FeO + MgO + TiO_2$ values indicate that the MMEs were generated by dehydration melting of a mafic lower crustal source. However, the host granitoids have higher $Al_2O_3/(FeO + MgO + TiO_2)$ ratios and lower $Al_2O_3 + FeO + MgO + TiO_2$ values, indicating a relatively felsic source or interaction with crustal rocks during intrusion or ascent from lower crustal regions. Given the wide range of inherited zircon ages, one might infer a mature sedimentary source.

The Tsushima granitoids exhibit a negative correlation in a Sr-Nd isotope plot (Fig. 6). In order to examine the possible role of assimilation and fractional crystallization (AFC) processes, data for basement

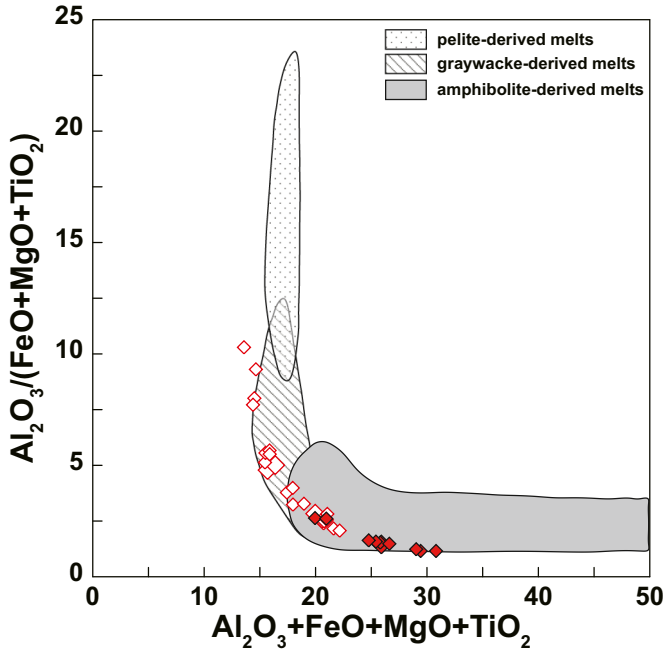

Fig. 8. Composition of the Tsushima granitoids and MMEs compared with the compositional fields of experimentally derived partial melts of metapelites, metagraywackes, and amphibolites. Data sources are from Douce (1999).

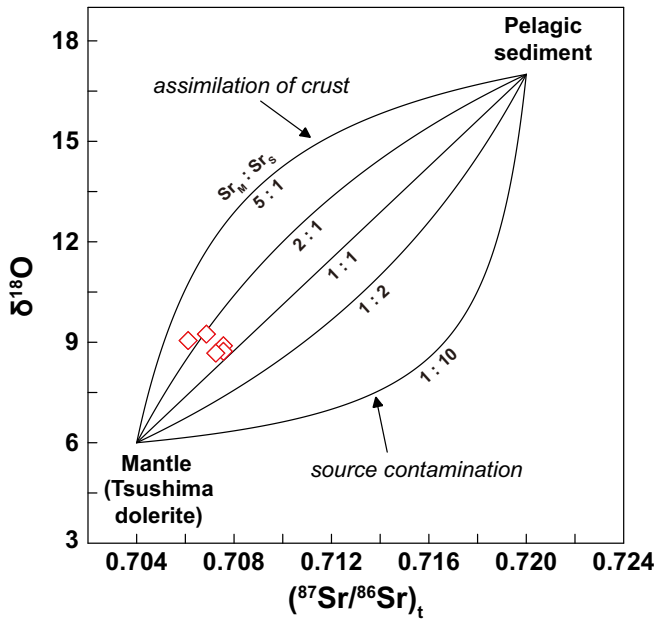

Fig. 9. Plot of $\delta^{18}O$ vs. initial $^{87}Sr/^{86}Sr$ for the Tsushima granitoids (after James, 1981). Theoretical two-component mixing curves for end-members comprising hypothetical mantle (M) and a contaminant (C) are shown for comparison. *M* is the composition of a Tsushima diabase ($\delta^{18}O$ = +6‰; $^{87}Sr/^{86}Sr$ = 0.7040) and *C* is the composition of pelagic sediment ($\delta^{18}O$ = +17‰; $^{87}Sr/^{86}Sr$ = 0.7200; Clayton et al., 1972; Cousens et al., 1994). Ratios shown alongside each curve denote the proportion of Sr from *M* (Sr_M) relative to that from *C* (Sr_S). Symbols are as in Fig. 3.

sedimentary rocks (Taishu Group) are shown in the Sr-Nd and Pb-Pb isotope diagrams (Figs. 6–7). The Taishu Group has highly radiogenic Sr and Pb, and unradiogenic Nd isotopic compositions, and forms the enriched end-member of the Tsushima granitoids in Sr-Nd and Pb-Pb isotope space (Figs. 6–7). We calculated a simple binary mixing curve between the least radiogenic Tsushima MME (Sr = 281 ppm; Nd = 18.7 ppm; $^{87}Sr/^{86}Sr = 0.7050$; $^{143}Nd/^{144}Nd = 0.51259$; Shin et al., 2009) and a representative Taishu Group rock (Sr = 148 ppm; Nd = 30.3 ppm; $^{87}Sr/^{86}Sr = 0.7161$; $^{143}Nd/^{144}Nd = 0.51199$; Shin et al., 2009) in Sr-Nd isotope space (Fig. 6). Some granitoids plot along the mixing curve, but there are also samples that fall away from the curve. Measured quartz $\delta^{18}O$ values of the Tsushima granites range from +8.7‰ to +9.3‰ (Table S4), which are within the range of published data for quartz from the Tsushima granitoids (+9.4‰ to +11.5‰; ±0.3‰ error; Ikemi et al., 2001). The whole-rock $\delta^{18}O$ values of the Tsushima granitoids range from +8.2‰ to +9.2‰, with an average of +8.7‰, which are much lower than those of the pelitic wall rocks in the Taishu Group (+14.2‰ to +14.7‰), thus ruling out significant crustal assimilation (Ishihara and Imai, 2000). The $\Delta^{18}O$ values between quartz and whole-rocks are +2‰ for coarse-grained and + 1‰ for fine-grained rocks (Trumbull et al., 2004). We note that the estimated $\delta^{18}O$ values are close to the average $\delta^{18}O$ value of the continental crust (8.9‰ ± 0.7‰; Simon and Lécuyer, 2005), suggesting a major crustal contribution to the granitic magmas. In addition, the Taishu Group generally plots between the MMEs and host granitoids on Harker diagrams (Figs. 4 and S5), ruling out the possibility of significant crustal assimilation during intrusion at shallow depths. Instead, the metasedimentary rocks must have been involved as source materials.

By using a combination of $\delta^{18}O$ and $^{87}Sr/^{86}Sr$ data, it is possible to assess the sources of the sedimentary rocks (i.e., subducted materials infiltrated into the mantle wedge vs. intracrustal rocks). Theoretical two-component mixing curves for $\delta^{18}O$ and $^{87}Sr/^{86}Sr$ are shown in Fig. 9. The two end-members are a mantle wedge as represented by the Tsushima diabases ($\delta^{18}O$ = +6‰; $^{87}Sr/^{86}Sr = 0.704$) and a pelagic sediment from the Pacific basin ($\delta^{18}O$ = +17‰; $^{87}Sr/^{86}Sr = 0.720$; Clayton et al., 1972; Cousens et al., 1994). Source contamination involves closed system partial melting of a mixture of crustal and mantle materials within the mantle (James, 1981). In contrast, the assimilation of crust represents crustal source hybridization or magma mixing at crustal levels (James, 1981). The Tsushima granitoids plot along the convex upward curve of the latter crustal level process. Also shown in the Sr-Nd and Pb-Pb isotope plots (Figs. 6–7) are available data for pelagic sediments from the East Sea (Sea of Japan), Philippine Sea, and abyssal plain east of Japan. These sediments have $^{143}Nd/^{144}Nd$ ratios similar to the Tsushima granites, but have more radiogenic Sr isotopic compositions and less radiogenic $^{207}Pb/^{204}Pb$ and $^{208}Pb/^{204}Pb$ at a given $^{206}Pb/^{204}Pb$, which rules out their presence as recycled materials in the mantle wedge. Instead, the Tsushima granitoids represent reworked crustal materials. Although the lower crust is dominated by mafic granulites that likely formed from basaltic underplating, it also includes diverse metasedimentary lithologies and evolved meta-igneous granulites (e.g., Rudnick and Gao, 2014). The presence of supracrustal assemblages at lower crustal depths is generally considered to result from thickening of the continental crust (e.g., Rudnick and Fountain, 1995).

In order to examine the possibility of hybrid source lithologies, multi-element modeling was conducted. The partition coefficients and concentrations of trace elements in the source materials (amphibolite and graywacke) and Taishu Group are given in Table S5. Modal fractional melting was used for the modeling. The results show that the Tsushima granitoids can be modeled as fractional crystallization of 60% Pl + 5% Kfs + 5% Qtz + 25% Amp +5% Bt ($f_{crystal} = 0.35$) from melts ($f_{melt} = 0.3$) derived from a hybrid source of amphibolite and graywacke ($f_{graywacke} = 0.3$; Fig. 10).

It is interesting to note that the Tsushima granitoids have more enriched Sr-Nd isotopic compositions than the MME samples, but indistinguishable Pb isotopic compositions. Fractionation in MMEs can be an open system process, whereby residual melts in the enclave may exchange, mix, or be replaced by melts from the granitoid host (Holden et al., 1991; Karsli et al., 2007). The mobility of Pb in an aqueous fluid is considerably higher than Sr or Nd (Kogiso et al., 1997). Notably, isotopic re-equilibration occurs even more rapidly than chemical diffusion (e.g.,

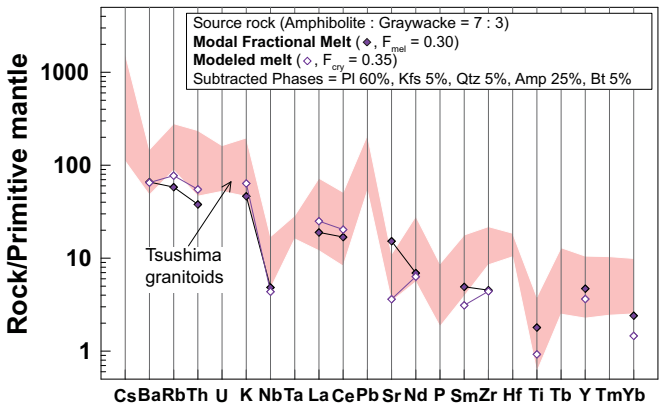

Fig. 10. Trace element concentrations of modeled melts after melting and crystallization processes. Detailed results of the modeling are listed in Table S5. Data sources: graywacke composition (35% Qtz + 30% Bt + 15% Plg + 5% Kfs + 15% Mc; Wedepohl, 1995); amphibolite composition (70% Amp + 30% Pl; Kogiso et al., 1997; Tatsumi, 2000). Abbreviations: F_{mel} = degree of melting; F_{cry} = degree of crystallization; Amp = amphibole; Bt = biotite; Kfs = K-feldspar; Mc = muscovite; Pl = plagioclase; Qtz = quartz.

Baker, 1989; Hofmann, 1980). Isotopic equilibrium for Pb can thus be achieved in the granite-MME system. Petrological evidence for the incorporation of crystals from the host granites into the Tsushima MMEs, such as ovoid quartz and overgrown plagioclase (Shin et al., 2009), independently support this hypothesis.

6.3. Tectonic implications

In the tectonic discrimination diagrams of Ti/100-Zr-Sr/2 and Ti/100-Zr-3 × Y (Pearce and Cann, 1973), the Tsushima diabases plot in the field for calc-alkaline basalt emplaced at convergent plate margins (Fig. 11a–b). They also plot in the calc-alkaline field in the Th/Yb vs. Ta/Yb diagram of Pearce (Pearce, 1982; Fig. 11c). They plot on the boundary between island arc basalts and mid-ocean ridge/within-plate basalts in a V vs. Ti/1000 discrimination diagram from Shervais (Shervais, 1982; Fig. 11d). The Eoil basaltic rocks from the Yangnam Basin also plot in the same fields as the Tsushima diabases (Fig. 11a-d).

The Tsushima granitoids fall in the field for I- and S-type granites in a plot of agpaitic index vs. Ga/Al ratio (Fig. 12a). In the Nb vs. Y tectonic discrimination diagram proposed by Pearce et al. (1984), most Tsushima granitoids plot in the volcanic arc/*syn*-collisional granite fields, but some samples plot in the within-plate granite field (Fig. 12b). On a Rb vs. Y + Nb classification diagram (Pearce, 1996; Pearce et al., 1984), the Tsushima granitoids plot within the post-collisional granitoid field (Fig. 12c). On the major element tectonic discrimination diagram of FeO(T)/[FeO(T) + MgO] vs. SiO_2, the Tsushima granitoids plot mostly in the field for arc-related granitoids, but some samples plot in the field for post-orogenic granitoids (Fig. 12d). In summary, the Tsushima plutons have geochemical characteristics of both subduction-related and within-plate settings.

These lines of evidence suggest a Miocene tectonic transition occurred in this area from a subduction-related to extensional setting. Extension in the East Sea could have caused thinning of the lithosphere and upwelling of the asthenosphere, which was possibly a subduction-modified mantle wedge, which then generated the Tsushima diabases

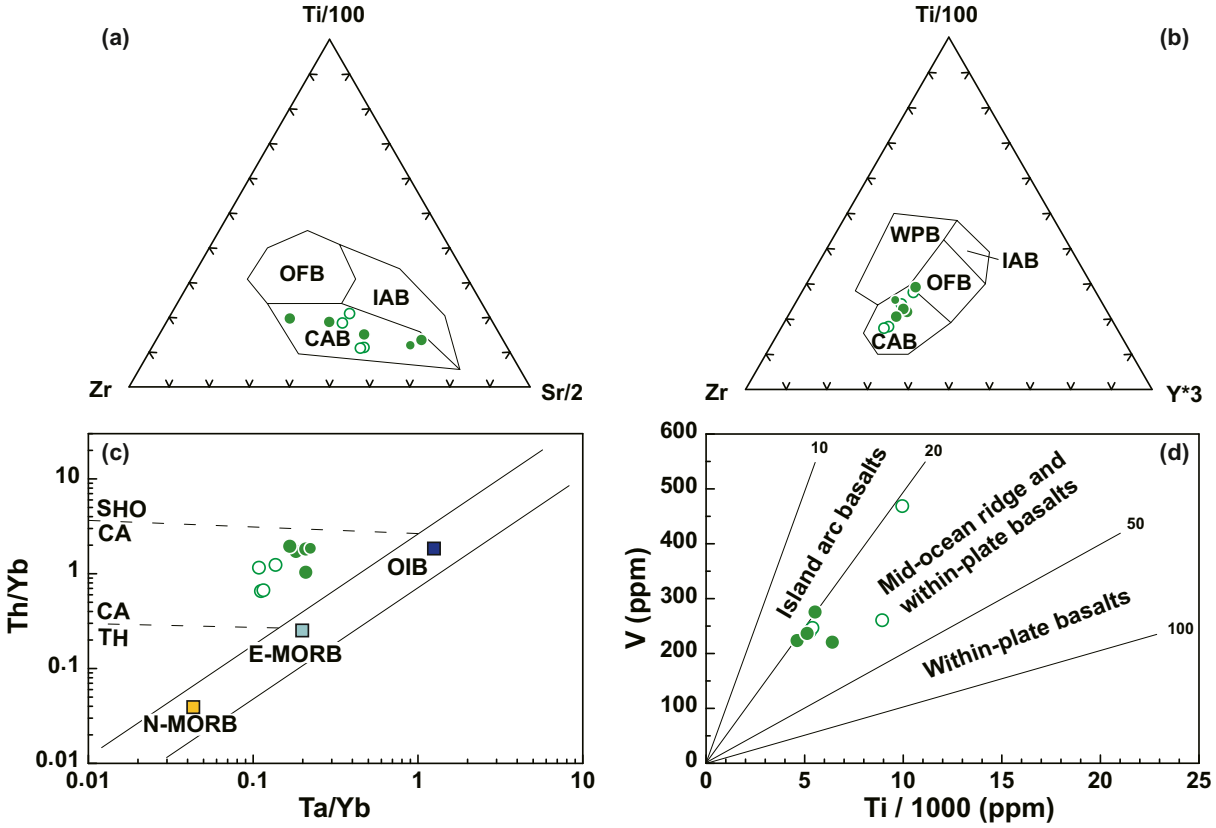

Fig. 11. Tectonic discrimination diagrams for the Tsushima diabases. Available data for Miocene basaltic rocks from the Yangnam Basin (Choi et al., 2013) are also shown for comparison. (a) Ti/100-Zr-Sr/2 and (b) Ti/100-Zr-3Y diagrams of Pearce and Cann (1973). (c) Th/Yb vs. Ta/Yb diagram of Pearce (1982). Dashed lines divide fields for SHO (shoshonite), CA (calc-alkaline), and TH (tholeiite). (d) V vs. Ti/1000 diagram of Shervais (1982). Abbreviations: OFB = ocean floor basalts; IAB = island arc basalts; CAB = calc-alkaline basalts; WPB = within-plate basalts; N- and *E*-MORB = normal and enriched mid-ocean ridge basalts, respectively; OIB = ocean island basalt. Symbols are as in Fig. 3.

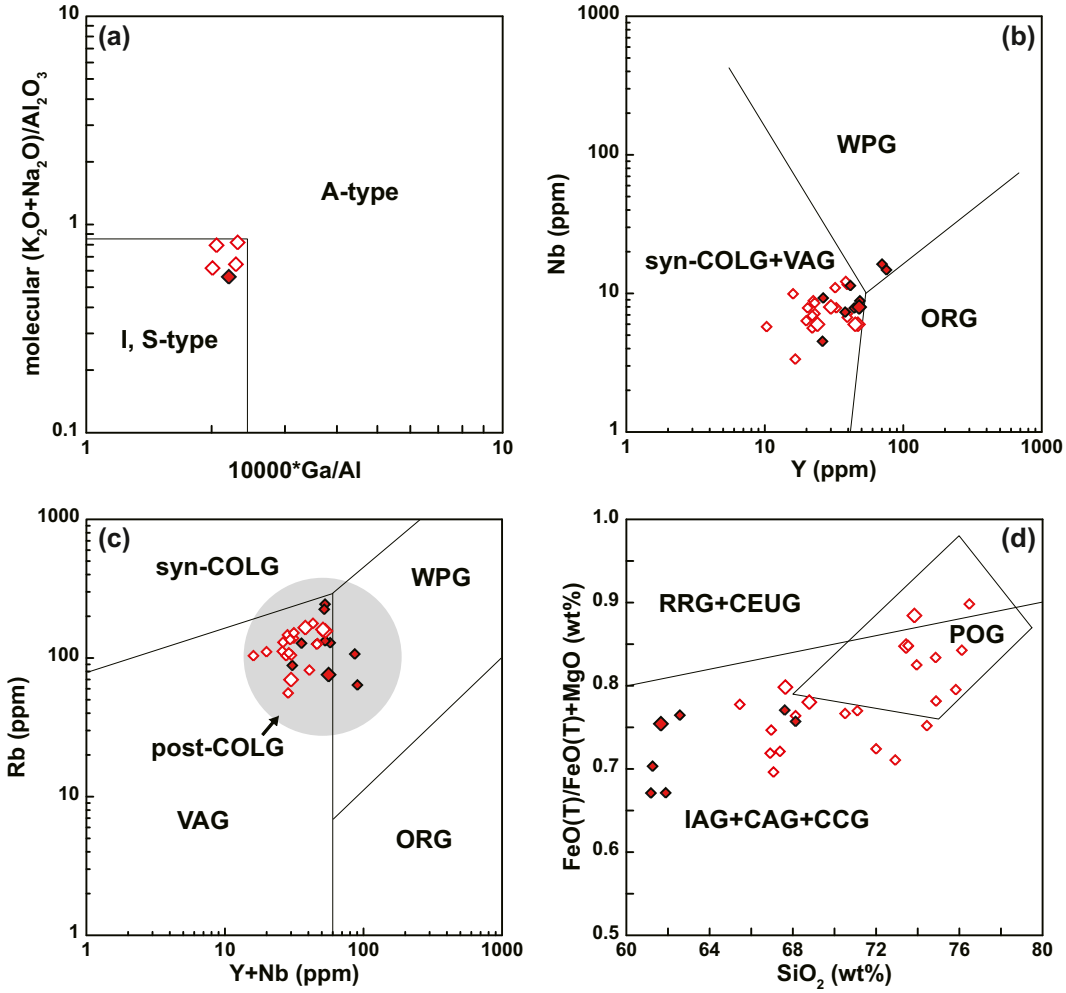

Fig. 12. Tectonic discrimination diagrams for the Tsushima granitoids. (a) Molar ($K_2O + Na_2O)/Al_2O_3$ vs. 10000Ga/Al diagram of Whalen et al. (1987), (b) Nb vs. Y diagram of Pearce et al. (1984), (c) Rb vs. (Y + Nb) diagram of Pearce et al. (1984) and Pearce (1996), and (d) FeO(T)/[FeO(T) + MgO] vs. SiO_2 diagram of Maniar and Piccoli (1989). Abbreviations: WPG = within-plate granitoids; *syn*-COLG = syn-collisional granitoids; ORG = ocean-ridge granitoids; VAG = volcanic-arc granitoids; post-COLG = post-collisional granitoids; IAG = island arc granitoids; CAG = continental arc granitoids; CCG = continental collision granitoids; POG = post-orogenic granitoids; RRG = rift-related granitoids; CEUG = continental epeirogenic uplift granitoids. Symbols and data sources are as in Figs. 3–4.

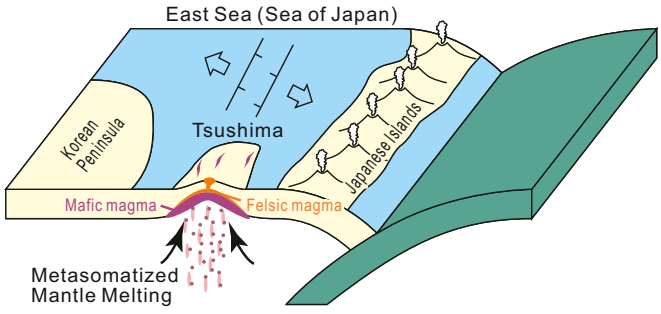

Fig. 13. A schematic illustration showing the Miocene melting processes beneath Tsushima Islands.

(Fig. 13). The asthenospheric upwelling might also have been the heat source for crustal melting and formation of the Tsushima granitoids (Fig. 13). The eastward extrusion of the Eurasian Plate induced by the India-Asia collision might have been the driving force for the extension (e.g., Peltzer and Tapponnier, 1988). The Tsuhima granitoids have flat HREE patterns (Fig. 5b), indicating a garnet-free source at pressures of <10 kbar (Douce, 1999; Rapp et al., 1991; Rapp and Watson, 1995). Emplacement at shallow levels in the crust is also evidenced by its thermal metamorphic aureole and porphyritic textures, and was related to the extensional tectonics.

7. Conclusions

(1) Zircon U-Pb data yield an age of 16.23 ± 0.16 Ma for a Tsushima granite. The granites contain MMEs.

(2) The coeval Tsushima diabases have arc-like depletions in HFSEs and enrichments in LILEs, and enriched Sr-Nd-Pb isotopic compositions compared with MORBs. However, they have normal mantle-like $\delta^{18}O_{clinopyroxene}$ values. These features and the transitional V-Ti systematics between an arc and non-arc setting indicate that upwelling in a subduction-modified mantle wedge might have generated the Tsushima diabases.

(3) The Tsushima granitoids have negative $\varepsilon_{Nd}(t)$ and $\varepsilon_{Hf}(t)$ values, enriched $(^{87}Sr/^{86}Sr)_t$ ratios, and continental crust-like $\delta^{18}O_{quartz}$ values, signifying reworking of an old crustal component. The occurrence of Paleoproterozoic to Jurassic inherited zircon cores also suggests the presence of mature sedimentary lithologies in the source. Multi-element modeling shows that the granitoids could have been produced by fractional crystallization of melts generated from a hybrid source of amphibolite and graywacke.

(4) The MMEs plot along the liquid line of descent of the granites. The diabases do not show coherent geochemical trends with the granites and MMEs, indicating they are not co-genetic. The MME has a more depleted Sr-Nd isotopic composition than the granites, but an indistinguishable Pb isotopic composition. The MME is considered to have formed by the partial melting of amphibolitic lower crust. Fractionation in the MME was likely to have been an open system process.
(5) The heating from asthenospheric upwelling might have induced crustal melting and formation of the Tsushima granitoids.

Declaration of Competing Interest

The authors declare that they have no known competing financial interests or personal relationships that could have appeared to influence the work reported in this paper.

Acknowledgements

This work was supported by the National Research Foundation of Korea (NRF) funded by the Korea Government (MSIT) (NRF-2019R1A2C1086666, NRF-2021R1A4A5026233). Insightful reviews by two anonymous reviewers greatly improved the manuscript. We thank Xian-Hua Li for the editorial handing.

Appendix A. Supplementary data

Supplementary data to this article can be found online at https://doi.org/10.1016/j.lithos.2021.106280.

References

Baker, D.R., 1989. Tracer versus trace element diffusion: diffusional decoupling of Sr concentration from Sr isotope composition. Geochim. Cosmochim. Acta 53, 3015–3023.
Choi, H.-O., Choi, S.H., Lee, D.-C., Kang, H.-C., 2013. Geochemical evolution of basaltic volcanism within the tertiary basins of southeastern Korea and the opening of the East Sea (Sea of Japan). J. Volcanol. Geotherm. Res. 249, 109–122.
Choi, S.H., 2021. Geochemistry and Petrogenesis of Quaternary Volcanic Rocks from Ulleung Island, South Korea. Lithos 380-381, 105874.
Choi, S.H., Mukasa, S.B., Kwon, S.T., Andronikov, A.V., 2006. Sr, Nd, Pb and Hf isotopic compositions of late Cenozoic alkali basalts in South Korea: evidence for mixing between the two dominant asthenospheric mantle domains beneath East Asia. Chem. Geol. 232, 134–151.
Chough, S.K., Kwon, S.-T., Ree, J.-H., Choi, D.K., 2000. Tectonic and sedimentary evolution of the Korean peninsula: a review and new view. Earth-Sci. Rev. 52, 175–235.
Clayton, R.N., Rex, R.W., Syers, J.K., Jackson, M.L., 1972. Oxygen isotope abundance in quartz from Pacific pelagic sediments. J. Geophys. Res. 77, 3907–3915.
Cousens, B.L., Allan, J.F., Gorton, M.P., 1994. Subduction-modified pelagic sediments as the enriched component in back-arc basalts from the Japan Sea: Ocean drilling program sites 797 and 794. Contrib. Mineral. Petrol. 117, 421–434.
Defant, M.J., Drummond, M.S., 1990. Derivation of some modern arc magmas by melting of young subducted lithosphere. Nature 347, 662–665.
Douce, A.E.P., 1999. What do experiments tell us about the relative contributions of crust and mantle to the origin of granitic magmas? Geol. Soc. Lond. Spec. Publ. 168, 55–75.
Eiler, J.M., Crawford, A., Elliott, T., Farley, K.A., Valley, J.W., Stolper, E.M., 2000. Oxygen isotope geochemistry of oceanic-arc lavas. J. Petrol. 41, 229–256.
Eiler, J.M., Farley, K.A., Valley, J.W., Hauri, E., Craig, H., Hart, S.T., Stolper, E.M., 1997. Oxygen isotope variations in ocean island basalt phenocrysts. Geochim. Cosmochim. Acta 61, 2281–2293.
Fabbri, O., Charvet, J., Fournier, M., 1996. Alternate senses of displacement along the Tsushima fault system during the Neogene based on fracture analyses near the western margin of the Japan Sea. Tectonophysics 257, 275–295.
Faure, M., Lalevée, F., 1987. Bent structural trends of Japan: Flexural-slip folding related to the Neogene opening of the Sea of Japan. Geology 15, 49–52.
Fisher, C.M., Vervoort, J.D., DuFrance, S.A., 2014. Accurate Hf isotope determinations of complex zircons using the "laser ablation split stream" method. Geochem. Geophys. Geosyst. 23, 121–139. https://doi.org/10.1002/2013GC004962.
Gonfiantini, R., 1978. Standards for stable isotope measurements in natural compounds. Nature 271, 534–536.
Hart, S.R., 1984. A large-scale isotope anomaly in the Southern Hemisphere mantle. Nature 309, 753–757.
Hofmann, A., 1980. Diffusion in silicate melts. In: Hargraves, R.B. (Ed.), Physics of Magmatic Processes. Princeton University Press, New York, pp. 385–417.
Holden, P., Halliday, A.N., Stephens, W.E., Henney, P.J., 1991. Chemical and isotopic evidence for major mass transfer between mafic enclaves and felsic magma. Chem. Geol. 92, 135–152.
Ikemi, H., Shimada, N., Chiba, H., 2001. Thermochronology for the granitic pluton related to lead-zinc mineralization in Tsushima, Japan. Resour. Geol. 51, 229–238.
Irvine, T.N.J., Baragar, W.R.A., 1971. A guide to the chemical classification of the common volcanic rocks. Can. J. Earth Sci. 8, 523–548.
Ishihara, S., Imai, A., 2000. Geneses of high chlorine and silver-lead-zinc-mineralized granitoids in Tsushima, Japan. Resour. Geol. 50, 169–178.
Ishikawa, N., Tagami, T., 1991. Paleomagnetism and fission-track geochronology on the Goto and Tsushima islands in the Tsushima strait area: implications for the opening mode of the Japan Sea. J. Geomagn. Geoelectr. 43, 229–253.
Itoh, Y., 2001. A Miocene pull-apart deformation zone at the western margin of the Japan Sea back-arc basin: implications for the back-arc opening mode. Tectonophysics 334, 235–244.
James, D.E., 1981. The combined use of oxygen and radiogenic isotopes as indicators of crustal contamination. Annu. Rev. Earth Planet. Sci. 9, 311–344.
Jolivet, L., Tamaki, K., 1992. Neogene kinematics in the Japan Sea region and volcanic activity of the northeast Japan arc. In: Proceedings of the Ocean Drilling Program, Scientific Results, 127/128, pp. 1311–1331. Part 2.
Karsli, O., Chen, B., Aydin, F., Şen, C., 2007. Geochemical and Sr-Nd-Pb isotopic compositions of the Eocene Dölek and Sariçiçek plutons, eastern Turkey: Implications for magma interaction in the genesis of high-K calc-alkaline granitoids in a post-collision extensional setting. Lithos 98, 67–96.
Kelemen, P.B., Hanghøj, K., Greene, A.R., 2003. One view of the geochemistry of subduction-related magmatic arcs, with an emphasis on primitive andesite and lower crust. In: Treatise on Geochemistry, vol. 3. Elsevier, pp. 593–659.
Kim, N.K., Kusakabe, M., Park, C., Lee, J.I., Nagao, K., Enokido, Y., Yamashita, S., Park, S.Y., 2019a. An automated laser fluorination technique for high-precision analysis of three oxygen isotopes in silicates. Rapid Commun. Mass Spectrom. 33, 641–649.
Kim, H.-G., Song, C.-W., Kim, J.-S., Son, M., Kim, I.-S., 2008. Tertiary geological structures and deformation history of the southern Tsushima Island, Japan. J. Geol. Soc. Korea 44, 175–198 (in Korean with English abstract).
Kim, S.W., Kwon, S., Santosh, M., Cho, D.-L., Kee, W.-S., Lee, S.-B., Jeong, Y.-J., 2019b. Detrital zircon U-Pb and Hf isotope characteristics of the early Neoproterozoic successions in the central-western Korean Peninsula: Implications for the Precambrian tectonic history of East Asia. Precambrian Res. 322, 24–41.
Kogiso, T., Tatsumi, Y., Nakano, S., 1997. Trace element transport during dehydration processes in the subducted oceanic crust: 1. Experiments and implications for the origin of oceanic island basalts. Earth Planet. Sci. Lett. 148, 193–205.
Kusakabe, M., Matsuhisa, Y., 2008. Oxygen three-isotope ratios of silicate reference materials determined by direct comparison with VSMOW-oxygen. Geochem. J. 42, 309–317.
Lallemand, S., Jolivet, L., 1985/1986. Japan Sea: a pull-apart basin? Earth Planet. Sci. Lett. 76, 375–389.
Le Maitre, R.W., Bateman, P., Dudek, A., Keller, J., Lameyre, J., Le Bas, M.J., Sabine, P. A., Schmid, R., Sorensen, H., Streckeisen, A., Woolley, A.R., Zanettin, B., 1989. A Classification of Igneous Rocks and Glossary of Terms. Blackwell, Oxford (206 p.).
Ludwig, K.R., 2008. User's Manual for Isoplot 3.6: a Geochronological Toolkit for Microsoft Excel. Berkeley Geochronology Center Special Publication, Berkeley.
Ludwig, K.R., 2009. User's Manual for SQUID 2. Berkeley Geochronological Center Special Publication, Berkeley.
McCulloch, M.T., Gamble, J.A., 1991. Geochemical and geodynamical constraints on subduction zone magmatism. Earth Planet. Sci. Lett. 102, 358–374.
Maniar, P.D., Piccoli, P.M., 1989. Tectonic discrimination of granitoids. Geol. Soc. Am. Bull. 101, 635–643.
Matsumoto, Y., Takahashi, K., 1987. Igneous activities in the Tsushima islands, Nagasaki Prefecture, Japan. Mono. Assoc. Geol. Collab. 33, 1–20.
Mattey, D., Lowry, D., Macpherson, C., 1994. Oxygen isotope composition of mantle peridotite. Earth Planet. Sci. Lett. 128, 231–241.
Otofuji, Y.-I., Itaya, T., Matsuda, T., 1991. Rapid rotation of Southwest Japan – paleomagnetism and K-Ar ages of Miocene volcanic rocks of Southwest Japan. Geophys. J. Int. 105, 397–405.
Otofuji, Y.-I., Matsuda, T., Nohda, S., 1985. Paleomagnetic evidence for the Miocene counter-clockwise rotation of Northeast Japan – rifting process of the Japan Arc. Earth Planet. Sci. Lett. 75, 265–277.
Paces, J.B., Miller Jr., J.D., 1993. Precise U-Pb ages of Duluth complex and related mafic intrusions, Northeastern Minnesota: geochronological insights to physical, petrogenic, paleomagnetic, and tectonomagmatic processes associated with the 1.1 Ga midcontinent rift system. J. Geophys. Res. Solid Earth 98, 13997–14013.
Paton, C., Hellstrom, J., Paul, B., Woodhead, J., Hergt, J., 2011. Ioite: Freeware for the visualization and processing of mass spectrometric data. J. Anal. At. Spectrom. 26, 2518.
Pearce, J.A., 1982. Trace element characteristics of lavas from destructive plate boundaries. In: Thorpe, R.S. (Ed.), Andesites: Orogenic Andesites and Related Rocks. John Wiley, New York, pp. 525–548.
Pearce, J.A., 1996. Sources and settings of granitic rocks. Episode 19, 120–125.
Pearce, J.A., Cann, J.R., 1973. Tectonic setting of basic volcanic rocks determined using trace element analyses. Earth Planet. Sci. Lett. 19, 290–300.
Pearce, J.A., Harris, N.B., Tindle, A.G., 1984. Trace element discrimination diagrams for the tectonic interpretation of granitic rocks. J. Petrol. 25, 956–983.
Peltzer, G., Tapponnier, P., 1988. Formation and evolution of strike-slip faults, rifts, and basins during the India-Asia collision: an experimental approach. J. Geophys. Res. 93, 15085–15117.

Perfit, M.R., Gust, D.A., Bence, A.E., Arculus, R.J., Taylor, S.R., 1980. Chemical characteristics of island-arc basalts: Implications for mantle sources. Chem. Geol. 30, 227–256.
Rapp, R.P., Watson, E.B., 1995. Dehydration melting of metabasalt at 8-32 kbar: Implications for continental growth and crust-mantle recycling. J. Petrol. 36, 891–931.
Rapp, R.P., Watson, E.B., Miller, C.F., 1991. Partial melting of amphibolite/eclogite and the origin of Archean trondhjemites and tonalities. Precambrian Res. 51, 1–25.
Rudnick, R.L., Fountain, D.M., 1995. Nature and composition of the continental crust: a lower crustal perspective. Rev. Geophys. 33, 267–309.
Rudnick, R.L., Gao, S., 2014. Composition of the continental crust. In: Treatise on Geochemistry, , Second ed.vol. 4. Elsevier, pp. 1–51.
Saitoh, Y., Ishikawa, T., Tanimizu, M., Murayama, M., Ujiie, Y., Yamamoto, Y., Ujiie, K., Kanamatsu, T., 2015. Sr, Nd, and Pb isotope compositions of hemipelagic sediment in the Shikoku Basin: Implications for sediment transport by the Kuroshio and Philippine Sea plate motion in the late Cenozoic. Earth Planet. Sci. Lett. 421, 47–57.
Shervais, J.W., 1982. Ti-V plots and the petrogenesis of modern and ophiolitic lavas. Earth Planet. Sci. Lett. 59, 101–118.
Shin, K.-C., Kurosawa, M., Anma, R., Nakano, T., 2009. Genesis and mixing/mingling of mafic and felsic magmas of back-arc granite: Miocene Tsushima pluton, Southwest Japan. Resour. Geol. 59, 25–50.
Simon, L., Lécuyer, C., 2005. Continental recycling: the oxygen isotope point of view. Geochem. Geophys. Geosyst. 6 https://doi.org/10.1029/2005GC000958.
Sun, S.S., McDonough, W.F., 1989. Chemical and isotopic systematics of oceanic basalts: implications for mantle composition and processes. Geol. Soc. Lond. Spec. Publ. 42, 313–345.
Takahashi, K., 1969. A study of the Taishu Group. Bull. Faculty Liberal Arts Nagasaki Univ. Nat. Sci. 10, 67–82.
Takahashi, K., 1992. Tsushima district. Geol. Japan 9, 120–123.
Takahashi, K., Hayashi, M., 1985. Fission track ages of igneous rocks from Tsushima Islands (I). Bull. Faculty Liberal Arts Nagasaki Univ. Nat. Sci. 25, 9–19 (in Japanese).
Takahashi, K., Hayashi, M., 1987. Fission track ages of igneous rocks from Tsushima Island (II). Bull. Faculty Liberal Arts Nagasaki Univ. Nat. Sci. 27, 19–21 (in Japanese).
Tatsumi, Y., 2000. Continental crust formation by crustal delamination in subduction zones and complementary accumulation of the enriched mantle I component in the mantle. Geochem. Geophys. Geosyst. 1 https://doi.org/10.1029/2000GC000094.
Tatsumi, Y., Hanyu, T., 2003. Geochemical modeling of dehydration and partial melting of subducting lithosphere: toward a comprehensive understanding of high-Mg andesite formation in the Setouchi volcanic belt, SW Japan. Geochem. Geophys. Geosyst. 4 https://doi.org/10.1029/2003GC000530.
Tatsumoto, M., Nakamura, Y., 1991. DUPAL anomaly in the Sea of Japan: Pb, Nd, and Sr isotopic variations at the eastern Eurasian continental margin. Geochim. Cosmochim. Acta 55, 3697–3708.
Trumbull, R.B., Harris, C., Frindt, S., Wigand, M., 2004. Oxygen and neodymium isotope evidence for source diversity in cretaceous anorogenic granites from Namibia and implications for A-type granite genesis. Lithos 73, 21–40.
Valley, J.W., 2003. Oxygen isotopes in zircon. Rev. Mineral. Geochem. 53, 343–385.
Vielzeuf, D., Clemens, J.D., Pin, C., Moinet, E., 1990. Granites, granulites, and crustal differentiation. In: Vielzeuf, D., Vidal, Ph. (Eds.), Granulites and Crustal Evolution, pp. 59–85.
Wedepohl, K.H., 1995. The composition of the continental crust. Geochim. Cosmochim. Acta 59, 1217–1232.
Whalen, J.B., Currie, K.L., Chappell, B.W., 1987. A-type granites: geochemical characteristics, discrimination and petrogenesis. Contrib. Mineral. Petrol. 95, 407–419.
Whalen, J.B., Jenner, G.A., Longstaffe, F.J., Robert, F., Gariéy, C., 1996. Geochemical and isotopic (O, Nd, Pb and Sr) constraints on A-type granite petrogenesis based on the Topsails igneous suite, Newfoundland Appalachians. J. Petrol. 37, 1463–1489.
Williams, I.S., 1998. U-Th-Pb geochronology by ion microprobe. In: McKibben, M.A., Shanks III, W.C., Ridley, W.L. (Eds.), Applications of Microanalytical Techniques to Understanding Mineralizing Processes. Reviews in Economic Geology, 7. Society of Economic Geologist, Socorro, pp. 1–35.
Zhao, Z.-F., Zheng, Y.-F., 2003. Calculation of oxygen isotope fractionation in magmatic rocks. Chem. Geol. 193, 59–80.
Zheng, Y.-F., 2019. Subduction zone geochemistry. Geosci. Front. 10, 1223–1254.
Zindler, A., Hart, S., 1986. Chemical geodynamics. Annu. Rev. Earth Planet. Sci. 14, 493–571.